Atomistic Study of Doped BaCeO3: Dopant Site-Selectivity and Cation Nonstoichiometry

ARTICLE *in* CHEMINFORM · JANUARY 2005

Impact Factor: 0.74 · DOI: 10.1021/cm048763z

4 AUTHORS, INCLUDING:

Richard Andrew Davies
Bangor University
19 PUBLICATIONS **501** CITATIONS
SEE PROFILE

M. Saiful Islam
University of Bath
173 PUBLICATIONS **7,232** CITATIONS
SEE PROFILE

Atomistic Study of Doped $BaCeO_3$: Dopant Site-Selectivity and Cation Nonstoichiometry

J. Wu,[†] R. A. Davies,[‡] M. S. Islam,*[,‡] and S. M. Haile*[,†]

Department of Material Science, California Institute of Technology, Pasadena, California 91125, and Materials Chemistry Group, Chemistry Division, University of Surrey, Guildford, GU2 5XH, UK

Received July 29, 2004. Revised Manuscript Received November 19, 2004

Rare earth (or yttrium) doped $BaCeO_3$ has been widely investigated as a proton conducting material. Usually, the trivalent dopants are assumed to occupy the Ce^{4+}-site, which introduces oxygen vacancies into the perovskite structure and furthers the protonic conductivity. Recent studies indicate the possibility of dopant incorporation on the Ba^{2+}-site, which is unfavorable for protonic conductivity. In this work atomistic simulation techniques, especially the supercell approach, have been developed to investigate the questions of dopant site-selectivity and cation nonstoichiometry in doped $BaCeO_3$. Our calculations predict that, on energetic grounds, Ba^{2+}-site deficiency shifts trivalent dopant incorporation onto the Ba^{2+}-site. These results confirm that the dopant partitioning or site-occupancy of trivalent dopants will be sensitive to the precise Ba/Ce ratio, and hence to the experimental processing conditions. The relative energies explain the experimentally observed "amphoteric" behavior of Nd with significant dopant partitioning over both Ba and Ce sites. Such partitioning reduces the concentration of oxygen vacancies, which, in turn, lowers proton uptake and decreases proton conductivity relative to dopant incorporation solely on the Ce^{4+} site.

Introduction

Doped barium cerate exhibits high proton conductivity upon exposure to humid atmospheres. In particular, Gd-doped $BaCeO_3$ exhibits a proton conductivity of 0.05 S/cm and a proton transference number of close to 1 at 600 °C.[1] These properties render doped barium cerate an attractive candidate for application in reduced-temperature solid oxide fuel cells and hydrogen sensors.[2−8]

To incorporate protons into the perovskite structure of barium cerate, doping by trivalent (M) species on the tetravalent (Ce) site is essential. Such doping generates oxygen vacancies ($V_O^{\bullet\bullet}$), eq 1, which, upon exposure to humid atmospheres, become filled with hydroxyl groups ($OH_O^{\bullet}$), eq 2,

$$2Ce_{Ce}^{x} + O_O^{x} + M_2O_3 \rightarrow 2M'_{Ce} + V_O^{\bullet\bullet} + 2CeO_2 \qquad (1)$$

$$H_2O(gas) + V_O^{\bullet\bullet} + O_O^{x} \rightarrow 2OH_O^{\bullet} \qquad (2)$$

where the reactions have been written in Kroger−Vink notation.[9] Water incorporation represented by eq 2, as shown, results in the uptake of two protons in the structure per oxygen vacancy. Thus, under ideal conditions, the oxygen vacancy concentration prior to humidification is $[V_O^{\bullet\bullet}] = {}^1/_2\,[M'_{Ce}]$, and the proton content after humidification is $[H^{\bullet}] = [M'_{Ce}]$. The concentration of Ce^{3+} is negligible under typical conditions.

To promote reaction 1 and attain the desired defect chemistry, materials are prepared with general stoichiometry $BaCe_{1-x}M_xO_{3-\delta}$ (where $\delta = {}^x/_2$). That is, the Ce content is lowered relative to the Ba content by an amount that corresponds to the dopant concentration. If some portion of the trivalent ions is incorporated onto the Ba^{2+}-site instead of the Ce^{4+}-site, dopant incorporation is described by eq 3

$$2Ba_{Ba}^{x} + M_2O_3 + V_O^{\bullet\bullet} \rightarrow 2M_{Ba}^{\bullet} + O_O^{x} + 2BaO \qquad (3)$$

In this case, oxygen vacancies are consumed instead of created, which prohibits the incorporation of hydroxyl groups in the subsequent hydration step. In a series of earlier studies,[10−12] extensive experimental evidence was presented that reaction 3 does take place in the case of large dopant cations. Dopant partitioning can occur such that a nonnegligible concentration of trivalent species resides on the Ba^{2+} site, lowering the concentration of oxygen vacancies to a value less than $[V_O^{\bullet\bullet}] = {}^1/_2\,[M'_{Ce}]$. Recent computational studies support a defect chemical model for M^{3+}-doped $A^{2+}B^{4+}O_3$ perovskites in which dopant partitioning over the two cation sites occurs on energetic grounds, and that the effect, perhaps predictably, is greatest for large dopant ions,

[†] California Institute of Technology.
[‡] University of Surrey.

(1) Taniguchi, N.; Haton, K.; Niikura, J.; Gamo, T.; Iwahara, H. *Solid State Ionics* **1992**, *53−56*, 998.
(2) Hibino, T.; Hashimoto, A.; Suzuki, M.; Sano, M. *J. Electrochem. Soc.* **2002**, *149*, A1503.
(3) Kruth, A.; Irvine, J. T. S. *Solid State Ionics* **2003**, *162−163*, 83.
(4) Song, S.; Wachsman, E.; Dorris, S.; Balachandran, U. *Solid State Ionics* **2002**, *149*, 1.
(5) Tomita, A.; Hibino, T.; Suzuki, M.; Sano, M. *J. Mater. Sci.* **2004**, *39*, 2493.
(6) Hui, Z.; Michele, P. *J. Mater. Chem.* **2002**, *12*, 3787.
(7) Coors, W.; Readey, D. *J. Am. Ceram. Soc.* **2002**, *85*, 2637.
(8) Maekawa, H.; Ukei, Y.; Morota, K.; Kashii, N.; Kawamura, J.; Yamamura, T. *Solid State Commun.* **2004**, *130*, 73.
(9) Kroger, F.; Vink, V. *Solid State Phys.* **1956**, *3*, 307.
(10) Shima, D.; Haile, S. M. *Solid State Ionics* **1997**, *97*, 443.
(11) Haile, S. M.; Staneff, G.; Ryu, K. H. *J. Mater. Sci.* **2001**, *36*, 1149.
(12) Wu, J.; Li, L. P.; Espinosa, W. P. T.; Haile, S. M. *J. Mater. Res.* **2004**, *19*, 2366.

10.1021/cm048763z CCC: $30.25
Published on Web 01/19/2005

because of the larger size of Ba^{2+} relative to Ce^{4+}.[13−15] This includes a combined EXAFS and simulation study of dopants in the $CaZrO_3$ proton conductor.[16]

The experimental studies further indicate that the extent to which dopant incorporation onto the Ba^{2+}-site occurs is tied to BaO loss at high temperature.[12] In the absence of dopants that can reside on the A site, the barium-deficient perovskite structure would either contain an excessively high concentration of vacancies on the Ba site, an energetically unfavorable situation, or precipitate out the CeO_2 fluorite phase; these two processes are illustrated, respectively, in eqs 4 and 5.

$$Ba_{Ba}^{x} + O_O{}^{x} \rightarrow V_{Ba}'' + V_O^{\bullet\bullet} + 2BaO\uparrow \quad (4)$$

$$Ba_{Ba}{}^{x} + Ce_{Ce}^{x} + 3O_O^{x} \rightarrow BaO\uparrow + CeO_2(ppt) \quad (5)$$

The latter reaction (that involving fluorite precipitation) has been observed experimentally for undoped barium cerate.[10] In the presence of dopant ions, it has been hypothesized that reaction 3 can occur, thereby stabilizing the perovskite phase against ceria precipitation.

In the present work we apply static lattice computational methods to directly investigate the defect chemistry of barium cerate on the atomic scale, and, in particular, the possible influence of cation nonstoichiometry on dopant site occupancy. Static lattice simulation methods have been successfully employed to investigate the defect properties of a range of perovskite-type proton and oxide-ion conductors.[13,14,17,18] Here, the particular trivalent dopant ions, Yb, Y, Gd, Nd and La, are examined.

2. Methodology and Problem Statement

Static lattice simulations are based on the specification of a potential model which describes the potential energy of the system as a function of the atomic coordinates and allows the modeling of both perfect and defective lattices. Only a brief account of these widely used techniques (embodied within the GULP code[17]) will be presented, as comprehensive reviews are given elsewhere.[18]

The Born model representation, commonly used for ternary oxides, is employed here, with the energy partitioned into long-range Coulombic and short-range pair (and three-body) potentials. A simple analytical function of the Buckingham form

$$V_{ij}(r_{ij}) = A_{ij}\exp(-r_{ij}/\rho_{ij}) - C_{ij}/r_{ij}^{6} \quad (6)$$

is used to describe the two-body, short-range interactions within the crystal, where V_{ij} is the potential energy between any two atoms i and j, A_{ij}, ρ_{ij}, and C_{ij} are the parameters describing the potential between those atoms, and r_{ij} is the distance between them.

Table 1. Interatomic Potential Parameters[a]

M···O	A (eV)	ρ (Å)	C (eV Å^6)	Y (e)	k (eV Å^{-2})	U_L (eV)	ref
O^{2-}	22764.30	0.1490	27.89*	−2.077*	27.29*		27
Ba^{2+}	931.7	0.3949	0.0	1.46	14.78	−31.33*	28
Ce^{4+}	1986.83	0.3511	20.40*	7.7	291.75	−105.31*	29
La^{3+}	1545.21	0.3590	0.0	−0.25	145.00	−129.06	27
Nd^{3+}	1379.9	0.3601	0.0	3.0	99999	−129.22	30
Gd^{3+}	1336.8	0.3551	0.0	3.0	99999	−132.16	30
Y^{3+}	1345.1	0.3491	0.0	3.0	99999	−134.74	30
Yb^{3+}	1309.6	0.3462	0.0	3.0	99999	−136.76	30

[a] A, ρ, and C are parameters assigned to the cation-oxide anion interaction, eq 6, Y is the shell charge, and k is the harmonic force constant, where Y and k are used in the shell model of ionic polarizability. U_L refers to the lattice energy of the oxide. Entries marked with an * are updated relative to ref 14.

As charged defects will polarize other ions in the lattice, ionic polarizability must be incorporated into the potential model. This is achieved using the shell model, which describes such effects by treating each ion in terms of a core (representing the nucleus and core electrons) connected via a harmonic spring to a shell (representing the valence electrons). The shell model has been shown to simulate effectively both dielectric and elastic properties of ceramic oxides, by including the vital coupling between the short-range repulsive forces and ionic polarization.[19,20] Values of the potential and shell model parameters for the species relevant to this work are listed in Table 1. The potentials for the trivalent dopant ions have been used successfully in previous work on perovskite oxides in which the Nd, Gd, Y, and Yb are effectively treated as rigid-ion species. An additional effect that must be treated is the lattice relaxation around a charged defect which causes extensive perturbation of the surrounding lattice. The phenomenon is modeled here using the two-region Mott−Littleton approach, which partitions the crystal lattice into two spherical regions. Ions in the central inner region (typically containing more than 250 ions) surrounding the defect are relaxed explicitly. In contrast, the remainder of the crystal (>2000 ions), where the defect forces are relatively weak, is treated by more approximate quasi-continuum methods. In this way, local relaxation is effectively modeled, and the crystal is not treated simply as a rigid lattice.

Although mean field theory, in which point defects are treated via a correction to the potential energy terms of particular atoms to generate an "average" or "hybrid" species, has been successful for treating defects in related systems[15] and even for the examination of other aspects of $BaCeO_3$,[14] this approach was found to be unsuitable here for a variety of reasons. Instead, a supercell approach has been implemented, with specific atom sites within the expanded cell (of overall symmetry $P1$) serving as the locations of particular point defects. As with other lattice simulations, the supercell is extended by periodic repetition in three dimensions to generate the full crystalline system.

(13) Buscaglia, M. T.; Buscaglia, V.; Viviani, M. *J. Am. Ceram. Soc.* **2001**, *84*, 376.
(14) Glockner, R.; Islam, M. S.; Norby, T. *Solid State Ionics* **1999**, *122*, 145.
(15) Davies, R. A.; Islam, M. S.; Gale, J. D. *Solid State Ionics* **1999**, *126*, 323.
(16) Davies, R. A.; Islam, M. S.; Chadwick, A. V.; Rush, G. E. *Solid State Ionics* **2000**, *130*, 115.
(17) Gale, J. D. *J. Chem. Soc., Faraday Trans.* **1997**, *93*, 629.
(18) Catlow, C. R. A. In *Solid State Chemistry: Techniques*; Cheetham, A. K., Day, P., Eds.; Clarendon Press: Oxford, 1987; Ch. 7.
(19) Dick, B.; Overhauser, A. *Phys. Rev.* **1958**, *112*, 90.
(20) Catlow, C. R. A.; Ackermann, L.; Bell, R.; Cora, F.; Gay, D.; Nygren, M.; Pereira, J.; Sastre, G.; Slater, B.; Sinclair, P. *Faraday Discuss.* **1997**, *106*, 1.

The supercell method presents its own set of challenges in that multiple defect configurations must be examined in order to identify that with the lowest energy. For example, for BaO deficiency with one cation vacancy on the barium site and one anion vacancy, the proximities of these two defects must be considered: as nearest neighbors, as next nearest neighbors, etc. To achieve a meaningful result within a finite time period, the strategy pursued here involved identification of the lowest energy configurations using relatively small supercells ($2 \times 2 \times 2$) and transferring these most probable configurations to progressively larger supercells. Final calculations were performed on $3 \times 4 \times 4$ and $3 \times 3 \times 5$ supercells. Introduction of two dopant ions within these supercells leads to dopant concentrations of ~4%, which are typical of experimental values.

The specific question that this work aims to answer is as follows: Given a nominal stoichiometry for a doped barium cerate perovskite, can the actual stoichiometry differ as a result of barium oxide evaporation (or accumulation in grain boundary regions) and dopant redistribution? The question can be formulated quantitatively in terms of the reaction

$$Ba(Ce_{1-x}M_x)O_{3-\delta} \rightarrow (Ba_{1-t}M_r)(Ce_{1-x}M_s)O_{3-\delta'} + tBaO \quad (7)$$

(where $r + s = x$). Is this reaction energetically favored, and to what extent do the thermodynamics depend on the particular dopant species?

In considering the stoichiometry of the barium-deficient composition, it is apparent that the degree of dopant incorporation onto the A-site determines the sign of the charge compensating defect. For $r < s$, negatively charged M'_{Ce} defects outnumber positively charged $M^{\bullet}_{Ba}$ defects, and oxygen vacancies are thus expected to be the primary type of compensating defect. For $r > s$, A-site vacancies (with negative charge) can be anticipated as the primary charge compensating defect. In either case, B-site vacancies are not anticipated. Calculation of the energetics of the complex perovskite, $(Ba_{1-t}M_r)(Ce_{1-x}M_s)O_{3-\delta'}$, presents computational challenges because of the multiple local configurations that must be considered in order to identify that which corresponds to the lowest energy. A simpler but equally valuable approach is to, instead, consider the energetics of the two extreme cases with the dopant entirely on one site or the other, and then calculate the energy of the reaction

$$Ba(Ce_{1-x}M_x)O_{3-\delta} \rightarrow [1-x](Ba_{1-y}M_{2y/3}V_{y/3})CeO_3 + zBaO \quad (8)$$

where V is a Ba vacancy, from the lattice energies of the three compounds, $Ba(Ce_{1-x}M_x)O_{3-\delta}$, $(Ba_{1-y}M_{2y/3}V_{y/3})CeO_3$, and BaO. Note that conservation of the dopant content requires $(1-x) \times {}^{2y}/_{3} = x$, whereas conservation of the mass of barium requires $1 = (1-x)(1-y) + z$.

In the ideal case, arbitrary values for x, y, and z can be examined. In a supercell of finite size, however, the stoichiometric variables are not continuous but rather have discrete values. Use of two different sized supercells addresses this limitation. Specifically, full Ce-site occupancy by the dopant is evaluated here using a $3 \times 4 \times 4$ supercell of composition $Ba_{48}(Ce_{46}M_2)O_{143}$ [$= Ba(Ce_{0.958}M_{0.042})O_{2.993}$], whereas full Ba-site occupancy is evaluated using a $3 \times 3 \times 5$ supercell of composition $(Ba_{42}M_2V_1)Ce_{45}O_{135}$ [$= (Ba_{0.933}M_{0.044})CeO_3$]. The specific reaction in this case then becomes

$$Ba_{48}(M_2Ce_{46})O_{143} \rightarrow {}^{46}/_{45}(Ba_{42}M_2V)Ce_{45}O_{135} + 5{}^{1}/_{15}BaO \quad (9)$$

and the total energy is calculated according to

$$\Delta E = 1.022E[(Ba_{42}M_2)CeO_3] + 5.067E[(BaO)] - E[Ba_{48}(M_2Ce_{46})O_{143}] \quad (10)$$

Note that due to compositional round-off errors, reaction 9 is not precisely mass balanced with respect to M_2O_3. However, this is a small error in light of other uncertainties in the calculation.

Table 2. Calculated Structural Parameters of Cubic $BaCeO_3$ as Determined from a Conventional $1 \times 1 \times 1$ Cell Calculation and Compared to Experimental Values

property	calculated	experimental[a]
lattice parameter a (Å)	4.427(2)	4.44467(2)
bond distances (Å)		
Ba−O	3.130(5)	3.143
Ce−O	2.213(6)	2.223
lattice energy (eV)	−136.68	

[a] Ref 31.

To facilitate comparisons with previous studies[14] we have also performed calculations in which the energetics of dopant substitution is calculated. The dopant cations are incorporated in the lattice at either the Ce^{4+} or Ba^{2+} sites represented by the defect reactions 1 and 3, or written more explicitly as

$$BaCeO_3 + xM_2O_3 \rightarrow Ba(Ce_{1-2x}M_{2x})O_{3-x} + 2xCeO_2 \quad (11)$$

and

$$BaCeO_3 + xM_2O_3 \rightarrow (Ba_{1-2x}M_{2x}V_x)CeO_3 + 3xBaO \quad (12)$$

respectively, (where reaction 12 is not entirely analogous to reaction 3, but is more appropriate for a direct comparison of site incorporation energies). The energies of these "solution" reactions are evaluated from the calculated lattice energies of the undoped and doped perovskite (using $3 \times 4 \times 4$ supercells and one formula unit M_2O_3 per 48 formula units $BaCeO_3$), and from the literature lattice energies of the binary oxides, U_L of Table 1. Analysis of the difference between the solution energies of these reactions, $\Delta E = E$(Ba-site) − E(Ce-site), provides a measure of the relative preference of the dopant for the Ce site over the Ba site and eliminates the influence of the lattice energies of the dopant metal oxides, which can overwhelm all other terms in the reaction.

In an earlier, related work,[14] studies of the defect chemistry of barium cerate were carried out using the mean field approach in conjunction with static lattice simulations. Three key results of that work are relevant to the present study: (1) the energetics of the cubic and orthorhombic forms of $BaCeO_3$ are almost identical; (2) for all dopants examined from Yb^{3+} to La^{3+}, incorporation onto the Ce site was found to be more favorable than onto the Ba site, but with the energy difference decreasing with increasing ionic radius; and (3) in undoped $BaCeO_3$, barium and oxygen vacancy

Table 3. Normalized Lattice Energy of Stoichiometric and Barium Oxide Deficient Barium Cerate in 3 × 4 × 4 and 3 × 3 × 5 Supercells, and Compared to the Values for the 1 × 1 × 1 Cell Calculation

cell		composition	lattice energy/unit cell (eV)	reaction energy[a] (eV)
$BaCeO_3$	1 × 1 × 1	$BaCeO_3$	−136.68	6.38
$Ba_{48}Ce_{48}O_{144}$	3 × 4 × 4	$BaCeO_3$	−136.68	}5.33
$Ba_{47}Ce_{48}O_{143}$	3 × 4 × 4	$Ba_{0.979}CeO_{2.979}$	−135.91	
$Ba_{45}Ce_{45}O_{135}$	3 × 3 × 5	$BaCeO_3$	−136.68	}5.54
$Ba_{44}Ce_{45}O_{134}$	3 × 3 × 5	$Ba_{0.978}CeO_{2.978}$	−135.86	

[a] For the formation of Ba and O vacancy pairs (see text, eq 14).

pairs created according to reaction 13 are the most energetically favorable intrinsic defects,

$$Ba_{Ba}^{x} + O_{O}^{x} \rightarrow V_{Ba}'' + V_{O}^{\bullet\bullet} + BaO \qquad (13)$$

although the total energy for even this reaction (6.4 eV) was found to be relatively high. This last result is consistent with the observation of A-site vacancies in perovskites such as $BaTiO_3$[21,22] and the loss of barium oxide from barium cerate based materials at elevated temperatures.[12] In the case of undoped barium cerate, however, compositions with just 1% deficiency (i.e., $Ba_{0.99}CeO_3$) result in two phase mixtures of the perovskite and ceria.[11,23] This suggests that any slight barium deficiency that is sustained in the undoped structure occurs at levels that cannot be easily detected experimentally, in accord with the computational result of rather high defect reaction energy. Here, in addition to evaluation of reaction 8 by the supercell approach, extensive computations on BaO deficient stoichiometries have been performed in order to assess the likelihood of barium loss via the reaction

$$BaCeO_3 \rightarrow Ba_{1-x}CeO_{3-x} + xBaO \qquad (14)$$

particularly in the presence of dopant ions. In the physical reality, BaO is likely to be removed in vapor form. However, calculations here were carried out assuming crystalline BaO, for which the lattice energy could be evaluated.

3. Results and Discussion

3.1 Structural Modeling and Intrinsic Defects of $BaCeO_3$. Before carrying out defect calculations, the unit cell dimensions and ion positions of the cubic phase ($Pm\bar{3}m$, a = 4.445 Å) were equilibrated under constant pressure at 0 K conditions using a 1 × 1 × 1 cell. The unit cell parameters change only slightly on relaxation of the structure. The differences in the observed and calculated lattice parameters and bond distances, Table 2, are within 0.4% for cubic $BaCeO_3$, indicating that the potentials reproduce the perovskite structure, although selected parameters are slightly updated from ref 14. Essentially identical structural results were obtained from the supercell calculations (in which, by definition, the structure was not constrained to be cubic). The energetics of intrinsic defect formation in (undoped) $BaCeO_3$ obtained from the 1 × 1 × 1 cell were, furthermore, within 5% of the earlier results[14] and are not reproduced here.

Table 4. Reaction Energy for the Creation of Ba and O Vacancy Pairs (eq 14) as Calculated Using 3 × 4 × 4 Supercells

dopant	reaction energy (eV)
none	5.33
La	5.98
Nd	6.47
Gd	6.69
Y	6.38
Yb	6.44

3.2 Dopant Incorporation. Before analyzing the defect chemistry of doped barium cerate, the consistency between the conventional 1 × 1 × 1 cell calculations and those of the supercells was checked by comparing lattice energies and Ba−O vacancy pair formation energies. The results, Table 3, show quantitative agreement in terms of lattice energies of stoichiometric compositions. In contrast, the supercell calculations (which are in good agreement with each other at a reaction energy of ∼5.4 eV) indicate defect creation energies which are somewhat lower than the conventional calculation using isolated point defects (∼6.4 eV). The difference reflects the likely influence of defect interactions. Such interactions are present in the supercell calculations but not the conventional calculations, which represent the dilute limit of isolated defects in an infinite crystal. If such an interpretation is correct, it further implies that barium cerate exhibits slightly nonideal solution behavior, with the chemical potential of defects being a function of defect concentration. Because of the uncertainties generally associated with lattice energy calculations, we focus on relative trends with respect to dopant type rather than the absolute energy values.

The energetics of Ba−O vacancy pair formation in the presence of dopant elements (on the B-site) for a 3 × 4 × 4 cell is presented in Table 4. Although there is no particular trend with ionic radius, it is apparent that the presence of B-site dopants raises the energetic penalty for the formation of these defects (from ∼5.3 eV to 6.0−6.7 eV). This result may be related to the nonideal solution behavior noted above, in which defect energy increases as the concentration of defects (in this case oxygen vacancies) increases.

The results of the dopant incorporation calculations are provided in Tables 5 and 6 and Figures 1 and 2. Specifically, the data in Table 5 and Figure 1 represent the results of the calculations based on reaction 9, whereas Table 6 and Figure 2 display the results in terms of reactions 11 and 12. The sign convention of Figure 2 is such that a positive value indicates preference for the Ce-site.

Examination of Figure 1 reveals that reaction 9, barium loss accompanied by simultaneous transfer of the dopant from the Ce to the Ba-site, is energetically unfavorable for small dopants, Yb, Y, and Gd, and becomes favorable as

(21) Yamada, A.; Chiang, Y. M. *J. Am. Ceram. Soc.* **1995**, *78*, 909.
(22) Brzozowski, E.; Castro, M. S. *J. Mater. Sci.: Mater. Electron.* **2003**, *14*, 471.
(23) Kreuer, K. D.; SchÖnherr, E.; Maier, J. *Solid State Ionics* **1994**, *70−71*, 278.

Table 5. Lattice Energies of Ba-Site and Ce-Site Doped Barium Cerate and the Energy for the Reaction[a]

cell	$3 \times 3 \times 5$	$3 \times 4 \times 4$		
formula	$(Ba_{42}M_2)Ce_{45}O_{135}$	$Ba_{48}(M_2Ce_{46})O_{143}$	reaction energy[a,b]	
composition	$(Ba_{0.933}M_{0.044})CeO_3$	$Ba(M_{0.042}Ce_{0.958})O_{2.993}$	ΔE (eV)	
dopant	eV/formula unit	eV/formula unit	reaction	form. unit
La	−137.29	−134.85	−1.1973	−0.025
Nd	−137.31	−134.91	0.5404	−0.011
Gd	−137.36	−134.97	1.6858	0.035
Y	−137.39	−135.02	2.4740	0.052
Yb	−137.43	−135.06	2.7351	0.057

[a] For the reaction $Ba_{48}(M_2Ce_{46})O_{143} \rightarrow 46/45(Ba_{42}M_2V)Ce_{45}O_{135} + (5^1/_{15})BaO$ [b] Total reaction energy is as calculated directly by $\Delta E = 1.022E[(Ba_{42}M_2)CeO_3] + 5.067E[(BaO)] - E[Ba_{48}(M_2Ce_{46})O_{143}]$. Energy per formula unit is normalized with respect to the starting material, $Ba_{48}(M_2Ce_{46})O_{143}$, by division by 48.

Table 6. Dopant Solution Energies in $BaCeO_3$ as Determined from of $3 \times 4 \times 4$ Supercells and Compared to Earlier Results Obtained Using the Mean Field Approximation

		Ce site (eV)/per dopant atom		Ba site (eV)/per dopant atom		ΔE [E(Ba-site) − E(Ce-site)] (eV)/per dopant atom	
dopant	ionic radius (Å)	supercell, rxn (11)	mean field [14]	supercell, rxn (12)	mean field[14]	supercell	mean field[14]
La	1.061	3.08	4.4	3.32	4.8	0.24	0.4
Nd	0.995	1.78	2.1	2.78	3.2	1.00	1.1
Gd	0.938	1.64	1.9	3.30	3.8	1.66	1.9
Y	0.900	1.81	1.9	3.88	4.3	2.07	2.4
Yb	0.858	1.80	2.0	4.31	4.7	2.51	2.7

the dopant ionic radius increases to La. The ionic radius dependence of the reaction energy is quite strong, spanning 4 eV for a dopant radius change of ∼0.2 Å. Although quantitative agreement with experimental data is not to be expected from these calculations, it is noteworthy that the

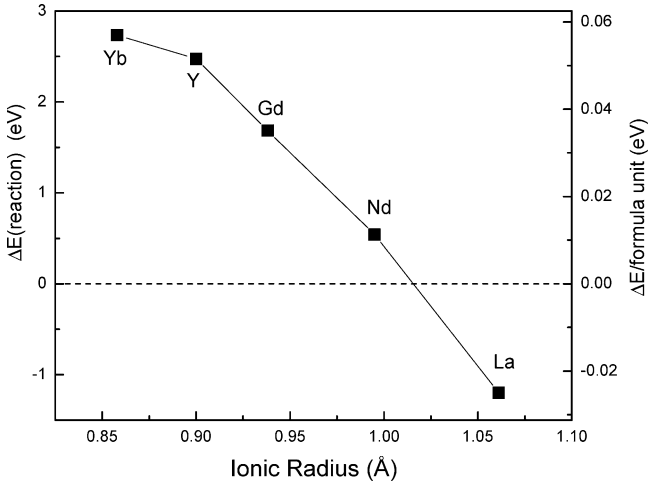

Figure 1. Energy of the reaction describing BaO loss and simultaneous transfer of trivalent dopant from Ce to the Ba site (reaction 9 in the text).

crossover point from positive to negative energy occurs at approximately Nd, a dopant for which measurable Ba-site occupation has been observed by experimental methods.[12] In particular, examination of $Ba_xCe_{0.85}M_{0.15}O_{3-\delta}$ (x = 0.85−1.20, M = Nd, Gd, Yb) materials has revealed the compositional limits for the maximum A-site incorporation to be as follows: $(Ba_{0.919}Nd_{0.081})(Ce_{0.919}Nd_{0.081})O_3$, $(Ba_{0.974}Gd_{0.026})(Ce_{0.872}Gd_{0.128})O_{2.875}$, and $Ba(Ce_{0.85}Yb_{0.15})O_{2.925}$.[12] Thus, Nd can be considered an "amphoteric" dopant with significant dopant partitioning over both Ba and Ce sites.

These results, along with the data in Table 4, further confirm that the site occupancy or dopant partitioning of trivalent dopants will be especially sensitive to the experimental processing conditions. In particular, loss of barium at high temperatures from (B-site) doped compositions produces relatively high energy Ba−O vacancy pairs and renders Ba-site occupancy by large dopants favorable. This would reduce the concentration of oxygen vacancies [via reaction 3] which, in turn, would lead to lower proton uptake [via reaction 2] and to a decrease in proton conductivity. Indeed, although a different interpretation was proposed, Kreuer et al.[24] reported a dramatic decrease in the conductivity of 10% Ba-deficient barium cerate doped with La upon prolonged exposure to high temperature. In more recent work, Shima and Haile showed proton uptake in Gd-doped barium cerate to decrease monotonically as the barium deficiency increased,[10] whereas Wu has observed similar behavior in Nd-doped barium cerate.[25]

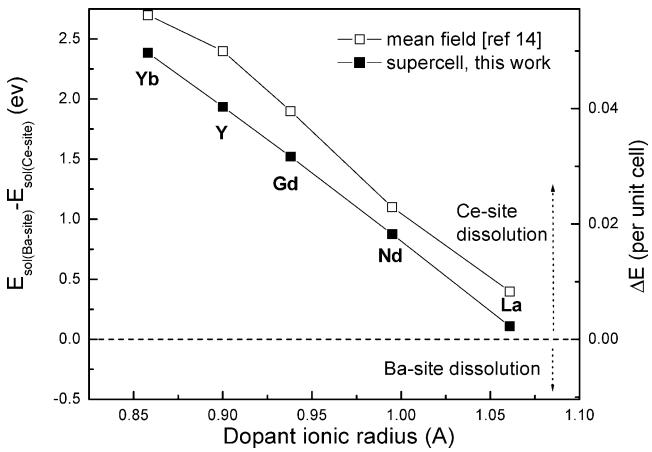

Figure 2. Solution energy of selected dopants into $BaCeO_3$.

Representation of the results in terms of reactions 11 and 12 in Figure 2 yields a similar ionic radius dependence as Figure 1, but with an overall apparent preference of all dopants examined, including even La, for the Ce site. As

(24) Kreuer, K. D.; SchÖnherr, E.; Maier, J. *Proc. 14th RisØ Intern. Sypm. on Materials Science*; RisØ National Laboratory: Roskilde, Denmark, 1993.

(25) Wu, J. Thesis: Defect Chemistry and Proton Conductivity in Ba-based Perovskites; California Institute of Technology: Pasadena, CA, 2004.

evident from Figure 2, the results obtained here by the supercell method are similar to those obtained earlier using the mean field approach,[14] but generally show a smaller energetic difference between incorporation on the two sites. As stated above, because of the uncertainties in the lattice energies, the relative trends in the solution energies are more meaningful than their absolute values and the discrepancies between the two calculations may not be significant. However, the difference between the two approaches embodied in Figures 1 and 2 warrants some discussion. Physically, what is represented in Figure 2 is the relative likelihood of initially stoichiometric barium cerate exsolving BaO or CeO_2 in order to accommodate isolated dopants on the Ba or Ce site at high dilution, respectively. Thus, the much larger lattice energy of CeO_2 over that of BaO, Table 1, encourages dopant dissolution on the Ce site accompanied by BaO exsolution, even for La, which otherwise has a preference for the Ba site.

4. Conclusions

Static lattice simulation techniques have been used to probe the defect chemistry of the proton conductor barium cerate. This study forms part of the continuing effort to improve our understanding of structure−composition−property relationships in ionic-conducting perovskites at the atomistic level. The simulations suggest that, on energetic grounds, the site-occupancy of dopants is linked to barium loss. Furthermore, while Ba−O vacancy pairs remain the most favorable intrinsic defect types, the energy of such defects increases upon introduction of B-site dopants. Thus, dopant redistribution over the A and B sites is energetically favorable over vacancy pair formation, and the dopant partitioning or site-occupancy of trivalent dopants will be sensitive to the precise Ba/Ce ratio and, hence, to the experimental processing conditions. The reaction energy for barium loss accompanied by simultaneous transfer of the dopant from the Ce to the Ba site is unfavorable for small dopants, Yb, Y, and Gd, and becomes favorable as the dopant ionic radius increases to La. The results for Nd point to "amphoteric" behavior with significant dopant partitioning over both Ba and Ce sites. Our results are consistent with the experimental compositional limits for A-site incorporation, which increases with increasing dopant ion radius.[12,26] Dopant incorporation onto the A-site has been shown to reduce the proton uptake and proton conductivity in doped barium cerate relative to the ideally B-site doped material, an affect that results from the reduction of the concentration of oxygen vacancies.

Acknowledgment. Funding of this work has been provided by the U.S. Department of Energy through the Office for Energy Efficiency and Renewable Energy. The visit of J.W. to Surrey was partly supported by the EPSRC.

CM048763Z

(26) Wu, J.; Webb, S.; Brennan, S.; Haile, S., *J. Appl. Phys.* In press.
(27) Khan, M. S.; Islam, M. S.; Bates, D. *J. Phys. Chem. B* **1998**, *102*, 3099.
(28) Lewis, G. V.; Catlow, C. R. A. *J. Phys. C: Solid State Phys.* **1985**, *18*, 1149.
(29) Balducci, G.; Islam, M. S.; Kapar, J.; Fornasiero, P.; Graziani, M. *Chem. Mater.* **2000**, *12*, 677.
(30) Freeman, C.; Catlow, C. R. A.. *J. Solid State Chem.* **1990**, *85*, 65.
(31) Knight, K. S. *Solid State Ionics* **1994**, *74*, 109.